ISSN 1674-1056
http://cpb.iphy.ac.cn
http://iopscience.iop.org/cpb
中国物理 B
Chinese Physics
中国物理 Chinese Physics B

Axial magnetic field effect in numerical analysis of high power Cherenkov free electron laser

F Bazouband, B Maraghechi

Citation: Chin. Phys. B . 2019, 28(6): 064101. **doi:** 10.1088/1674-1056/28/6/064101
Journal homepage: http://cpb.iphy.ac.cn; http://iopscience.iop.org/cpb

What follows is a list of articles you may be interested in

Modulation of absorption manner in helicon discharges by changing profile of low axial magnetic field

Gao Zhao(赵高), Yu Wang(王宇), Chen Niu(牛晨), Zhong-Wei Liu(刘忠伟), Jiting Ouyang(欧阳吉庭), Qiang Chen(陈强)
Chin. Phys. B . 2017, 26(10): 105201. **doi:** 10.1088/1674-1056/26/10/105201

Tunable terahertz radiation from arbitrary profile dielectric grating coated with graphene excited by an electron beam

Zhao Tao, Zhong Ren-Bin, Hu Min, Chen Xiao-Xing, Zhang Ping, Gong Sen, Liu Sheng-Gang
Chin. Phys. B . 2015, 24(9): 094102. **doi:** 10.1088/1674-1056/24/9/094102

Effects of self-fields on electron trajectory and gain in planar wiggler free-electron lasers with two-stream and ion-channel guiding

S. Saviz, M. Karimi
Chin. Phys. B . 2014, 23(3): 034103. **doi:** 10.1088/1674-1056/23/3/034103

Effects of self-fields on gain in two-stream free electron laser with helical wiggler and an axial guiding magnetic field

Saviz S, Lashani E, Ashkarran A
Chin. Phys. B . 2014, 23(2): 024102. **doi:** 10.1088/1674-1056/23/2/024102

Investigation of intense sheet electron beam transport using the macroscopic cold-fluid model and the single-particle orbit theory

Han Ying,Ruan Cun-Jun
Chin. Phys. B . 2012, 21(5): 054103. **doi:** 10.1088/1674-1056/21/5/054103

Axial magnetic field effect in numerical analysis of high power Cherenkov free electron laser

F Bazouband[1,†] and B Maraghechi[2]

[1] *Department of Physics, Fasa University, Post code* 74616 – 86131, *Fasa, Iran*
[2] *Department of Physics, Manhattanville College, Purchase, New York* 10577, *USA*

(Received 27 October 2018; revised manuscript received 24 February 2019; published online 29 May 2019)

Cherenkov free electron laser (CFEL) is simulated numerically by using the single particle method to optimize the electron beam. The electron beam is assumed to be moving near the surface of a flat dielectric slab along a growing radiation. The set of coupled nonlinear differential equations of motion is solved to study the electron dynamics. For three sets of parameters, in high power CFEL, it is found that an axial magnetic field is always necessary to keep the electron beam in the interaction region and its optimal strength is reported for each case. At the injection point, the electron beam's distance above the dielectric surface is kept at a minimum value so that the electrons neither hit the dielectric nor move away from it to the weaker radiation fields and out of the interaction region. The optimal electron beam radius and current are thereby calculated. This analysis is in agreement with two previous numerical studies for a cylindrical waveguide but is at odds with analytical treatments of a flat dielectric that does not use an axial magnetic field. This is backed by an interesting physical reasoning.

Keywords: Cherenkov free electron laser, axial magnetic field, flat dielectric slab, electron beam

PACS: 41.60.Cr, 52.59.Rz, 41.60.Bq, 41.85.Lc **DOI:** 10.1088/1674-1056/28/6/064101

1. Introduction

Terahertz (THz) radiation, due to its unique properties, has found to possess numerous applications in various branches, such as science, industry, medicine, and military/security.[1,2] One of the sources of THZ radiation is Cherenkov free electron laser (CFEL) which is capable of producing wavelengths in the range from sub-millimeters to infrared.[3–8] In the CFEL, the coupling of the electron beam that is moving near the surface of a dielectric to its Cherenkov radiation,[9] leads to the amplification of the coherent radiation in the interaction region.[10–14] Different arrangements of CFELs including single slab dielectric,[15,16] double slab dielectric layers,[17] CFEL in an asymmetric dielectric liner waveguide,[18] and cylindrical dielectric[19,20] have been studied. Also Cherenkov radiation oscillator without reflectors in which an electron beam travelled over a finitely thick plate made of negative-index material was studied in Ref. [21] and its dispersion equation, spatial growth rate, and start current were analyzed.[22,23] In Ref. [24], a CFEL with metallic side walls was proposed. Small-signal gain of Cherenkov radiation generated by hot electrons in the collective regime was studied in Ref. [25]. A novel type of slow-wave structure for Smith–Purcell FEL is developing as a high power, tunable and compact THz radiation source. A dielectric loaded metal grating for Smith–Purcell device was proposed in Refs. [26] and [27]. A way of realizing an integrated free electron laser in the ultraviolet frequency region was presented by discovering the surface plasmon amplification.[28] The experimental facility and measurement of the power and frequency spectrum of high power THz FEL were reported in Refs. [29] and [30], and the averaged power of 20 mW was shown at first experiments. A THz CFEL driven by an MeV picosecond electron beam was presented numerically in Ref. [31].

Over the past few decades, several efforts have been made to generate the coherent radiation from CFEL for a wide range of output power and electron beam energy. An experimental investigation of a compact and economical CFEL driven by a high-quality low-energy electron beam (150 keV) reported in Ref. [32] has a strong gain but a remarkably low output power (PW). The generation of coherent emission from CFEL driven by 5-MeV electron beam and output power up to 50W was described in Ref. [4]. The interaction of a mildly relativistic electron beam (400 kV) with the Cherenkov radiation that produced output power of 500 kW at 150 GHz was experimentally reported in Ref. [7]. A theoretical description of the CFEL operating in the high-gain regime is developed in a wavelength range from the far infrared to submillimeter in Ref. [6]. A numerical simulation[33] complements the experimental development[34] of a dielectric Cerenkov maser amplifier operating with a beam voltage of 890 kV and current of 300 A and total output power of 30 MW at a frequency of 8.7 GHz.

Asgekar and Dattoli in 2002 presented a fully equivalent formalism to study the Cherenkov and undulator high gain free electron laser (FEL) dynamics.[35] In a separate study they also obtained the saturation intensity of CFEL oscillator by using

†Corresponding author. E-mail: fbazooband@gmail.com

© 2019 Chinese Physical Society and IOP Publishing Ltd

pendulum-like equations.[10] The roots of the dispersion relation in the absence of the electron beam were used in Ref. [32] to find the growth rate of the radiation and to present an analysis for a single slab CFEL driven by a flat electron beam. A unified theoretical analysis of the spontaneous and stimulated emission was presented in Ref. [36].

In 1996, the single slab CFEL was simulated based on a model in terms of the radiation phase and electron energy.[16] However, they did not consider the facts that the electric and magnetic fields varied over the beam cross-section and that the beam changed its distance from the dielectric surface. No axial magnetic field was also considered. In 1990 the numerical investigation of the nonlinear evolution of CFEL for the cylindrical waveguide with a dielectric lining was presented.[20] By including an axial magnetic field, good agreement between the theory and experiment was reported. However, the trajectories of the electrons were not discussed.

In most of the theoretical studies of CFEL a focusing axial magnetic field has not been considered[10,15,16,35,37,38] and this might pose a problem because in the absence of a focusing mechanism the electrons could either move away from the dielectric slab, leaving the interaction zone with the radiation, or got closer to it and strike the dielectric. In the theoretical investigation of a low power CFEL in Ref. [39], an axial magnetic field for the focusing of the electron beam was discussed but its effect on the dynamics of the beam has not been considered. This is of a greater importance in the case of high power CFEL with a flat dielectric slab,than in the case of the cylindrical dielectric waveguide, because of its strong asymmetric nature. There is a flat dielectric slab on one side of the electron beam and vacuum on the other side. This makes the electron beam susceptible to drift in one direction or the other, thereby jeopardizing the interaction.

The purpose of the present investigation is to use the single particle analysis of CFEL with a dielectric slab and a focusing axial magnetic field to find out how the electron beam behaves as it moves through the growing radiation. Three different cases of the electron beam energy and the radiation growth are considered. It is found that in the flat dielectric CFEL with high output power, the presence of a strong axial magnetic field is a necessity and the position where the electron beam is injected is of great importance. In all cases without axial magnetic field, the radiation is not amplified into large output power, because the electrons either hit the dielectric or move away from the interaction region, thereby disrupting the interaction.

The organization of the rest of this paper is as follows. In Section 2, the basic geometry of the CFEL configuration is presented and formulations for electron dynamics are obtained by using the Lorentz-force equations. In Section 3, numerical results are presented and concluding remarks are made in Section 4.

2. General formulation

The CFEL, considered in this analysis and shown in Fig. 1, consist of a flat dielectric with thickness d and the dielectric constant ε, which is coated on a conductive surface. The electron beam with a circular cross-section and radius r_b is injected along the z direction at $z = 0$. In this investigation, the motion of three separate points (electrons) of a circular electron beam is studied using the single particle analysis. The evolution of the electron beam is determined by the displacement of these three representative points with respect to the dielectric surface. The characteristics of the electromagnetic radiation propagating along the z direction can be found by solving the Maxwell's equations and imposing the boundary conditions, which yield the following equations for the vector potential of the transverse magnetic (TM) mode outside the dielectric at $x > d$:

$$\delta A_z(z) = \delta A(z) \sin qd\, \mathrm{e}^{-p(x-d)} \sin(\kappa z - \omega t), \tag{1}$$

$$\delta A_x(z) = \delta A(z) \frac{\kappa \sin qd}{p}\, \mathrm{e}^{-p(x-d)} \cos(\kappa z - \omega t). \tag{2}$$

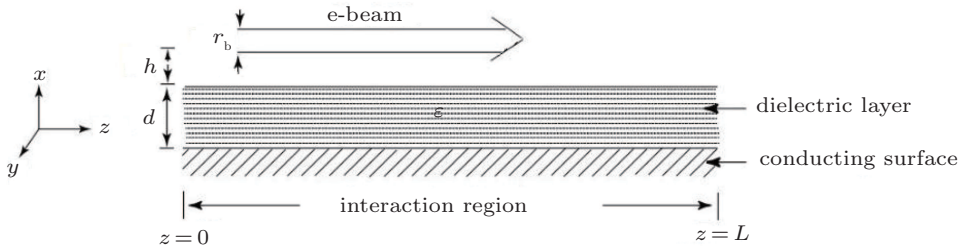


Fig. 1. Schematic diagram of single slab CFEL.

Here, $p = \sqrt{\kappa^2 - \omega^2/c^2}$ and $q = \sqrt{\varepsilon\omega^2/c^2 - \kappa^2}$ with κ and ω being the wave number and frequency of the radiation, respectively. The dispersion relation is given by $q\tan(qd) = \varepsilon p$, which defines the spectrum of radiation in the CFEL, *i.e.*, how ω changes with κ. However the amplification of radiation in CFEL is only possible for the resonant frequency and the corresponding wavelength, which can be found by simultaneous solution of the above dispersion relation and the syn-

chronism condition. Under synchronism condition the phase velocity of the radiation is equal to the electron beam velocity. The resonant interaction of the electron beam with the radiation leads to its coherent amplification with the growth rate Γ expressed by $\delta A(z) = \delta A_0 \exp[\Gamma z]$.

By using the Lorentz-force equation of motion, the relativistic equation of motion of a single electron in the electromagnetic fields of the radiation and confining axial magnetic field B_0 along the z direction can be found to be,

$$\frac{\mathrm{d}u_x}{\mathrm{d}z} = \frac{e\omega}{m_e c^2}\left(\frac{\omega\,\kappa\,\sin qd}{p\,v_z}\sin\alpha_+ + \frac{\omega^2\,\sin qd}{p\,c^2}\sin\alpha_+ + \frac{\kappa\,\sin qd}{p\,v_z}\Gamma(z)\cos\alpha_+\right)\delta A(z)\,\mathrm{e}^{-p(x-d)} - \frac{eB_0}{m_e c^2}\frac{v_y}{v_z}, \quad (3)$$

$$\frac{\mathrm{d}u_y}{\mathrm{d}z} = \frac{-eB_0}{m_e c^2}\frac{v_x}{v_z}, \quad (4)$$

$$\frac{\mathrm{d}u_z}{\mathrm{d}z} = \left(-\frac{e}{m_e c^2}\frac{v_x}{v_z}\left[\frac{\omega^2\sin qd}{p\,c^2}\sin\alpha_+ + \frac{\kappa\sin qd}{p}\Gamma(z)\cos\alpha_+\right] + \frac{e\,\omega}{m_e c^2\,v_z}\sin qd\cos\alpha_+\right)\delta A(z)\,\mathrm{e}^{-p(x-d)}, \quad (5)$$

$$\frac{\mathrm{d}x}{\mathrm{d}z} = \frac{v_x}{v_z}, \quad (6)$$

$$\frac{\mathrm{d}y}{\mathrm{d}z} = \frac{v_y}{v_z}, \quad (7)$$

$$\frac{\mathrm{d}\alpha_+}{\mathrm{d}z} = k - \frac{\omega}{v_z}. \quad (8)$$

Here, $\alpha_+ = \kappa z - \omega t$ and $\boldsymbol{u} = \gamma\boldsymbol{v}$ with γ being the relativistic factor of the electron beam. Also the relation $\mathrm{d}/\mathrm{d}t = v_z\,\mathrm{d}/\mathrm{d}z$ is used to change the differentiation from t to z.

In the present analysis, the single particle theory of a CFEL is used to find out how the electron beam behaves and develops as radiation grows. The radiation is assumed to grow, in an amplifier mode, with a constant growth rate and a saturated power which are taken from experimental measurements and simulations. The assumed structure supports TM modes which are tuned at the resonant frequency by using the dispersion relation, so their characteristics are prevailed throughout the interaction region. The study of the trajectories of the electrons is of vital importance in two regards. On the one hand, if the electron beam is injected too close to the dielectric surface, too many of the electrons might hit the dielectric slab. On the other hand, if they are injected too far from the dielectric surface, the Cherenkov effect will be weakened by diminishing electromagnetic fields of the radiation by the factor $\exp[-p(x-d)]$ as we move away from the dielectric surface. Using the present single particle analysis, optimum values for the injection height and the beam radius can be found. For this purpose, we require that the upper part of the electron beam, *i.e.*, the electron with the largest distance above the dielectric surface experiences 30% reduction in the electromagnetic field's amplitude. 30% reduction at the top of the beam is chosen so the radiation inside the electron beam would not be attenuated profoundly. So we should have $\exp[-p(x_{\max}-d)] = 0.7$ where $x_{\max}$ is the position of the electron at the top of the electron beam with a largest distance from the dielectric surface. This will yield $x_{\max} = d + 0.36/p$ where $1/p$ is the characteristic distance for which field's amplitudes will be reduced by 32% and depends on the resonant frequency.

3. Numerical results and discussion

Equations (3)–(8) form a set of first order coupled differential equations that will be solved numerically by using the fourth-order Runge–Kutta method, subject to the following initial conditions imposed on the single electron of the beam,

$$y(z=0) = 0, \quad x(z=0) = d + h,$$
$$u_x(z=0) = u_y(z=0) = 0, \quad u_z(z=0) = \sqrt{\gamma_0^2 - 1}, \quad (9)$$

where γ_0 is the initial energy of the beam and h is the electron's initial distance from the dielectric surface. The space-charge effect, *i.e.*, Coulomb effect is neglected since $\omega_{\mathrm{p}} \ll \omega$, where ω is the resonant frequency that can be found by assuming synchronism between the electron beam and the radiation, and $\omega_{\mathrm{p}}(=\sqrt{4\pi n_{\mathrm{b}}\,\mathrm{e}^2/m_{\mathrm{e}}c^2})$ is the plasma frequency of the electron beam. One important implication of the space-charge effect of a high density electron beam is its self-electric field that works to expand and de-focus the beam. The strong axial magnetic field that we find to be necessary in order to confine the electrons to the interaction zone has actually another important effect that is opposite to the self-electric field and tries to keep the electron beam focused.[40] Although CFELs operate with relatively high density electron beams, in this analysis the electron beam density is considered to be at the lower end so the space-charge effects can be neglected because of $\omega_{\mathrm{p}} \ll \omega$. For higher densities, however, the problem can be easily generalized to include the self-electric and magnetic fields of the relativistic electron beam, thereby the space-charge effect is taken into account. Three separate cases corresponding to different beam energy and saturated power of the radiation will be studied. The absorption loss of the dielectrics considered in this study is negligible in the THz regime.[41]

3.1. Low beam energy and low radiation growth

The first set of parameters corresponds to a computer simulation in Ref. [20] and the relevant experiment in Ref. [5]. These studies were performed for a cylindrical waveguide with a dielectric lining and employed an axial magnetic field for the beam focusing. We use a flat dielectric slab instead but with the same material boron nitride of $\varepsilon = 4.2$. The beam energy is 150 keV which corresponds to $\gamma_0 = 1.29$. The resonant frequency for the cylindrical waveguide[20] was 104 GHz.

Here, for the flat dielectric the same resonant frequency is obtained for the dielectric thickness of $d = 450$ μm. Also in Ref. [20], the initial power of 10 W was grown exponentially to the saturation power of 10^4 W over the distance of 18 cm, for the cylindrical waveguide. The corresponding vector potential $\delta a (= e\delta A/mc^2)$ that grows exponentially like $\delta a = \delta a_0 \exp[\Gamma z]$ with the growth rate $\Gamma = 0.011$ (1/cm) is shown in Fig. 2(a). We expect the trajectory of electrons to change as the beam moves ahead along with the growing radiation.

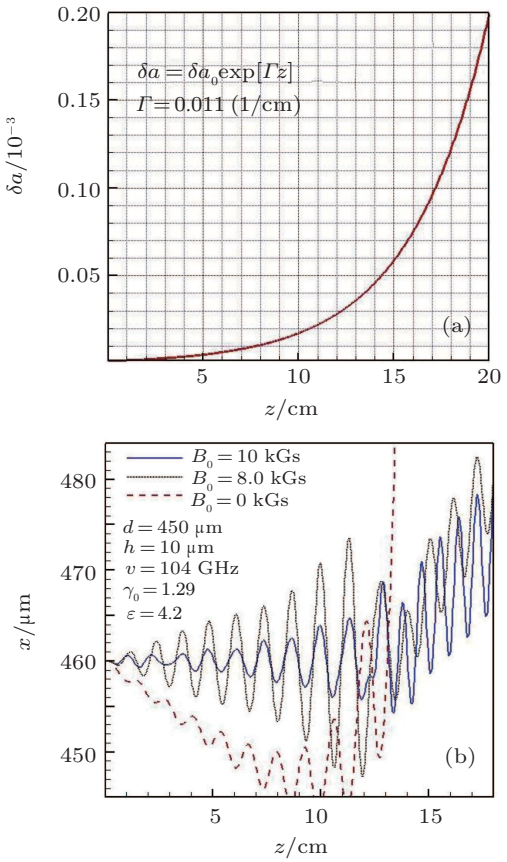


Fig. 2. (a) Exponential variation of vector potential along z axis with growth rate $\Gamma = 0.011$ (1/cm), and (b) x–z position of the lower part of the beam for different values of axial magnetic field.

Figure 2(b) shows that the variations of the x position of the lower part of the beam along the z axis as it moves through the radiation along the z axis, for different values of the axial magnetic field. This electron is injected at $x_{\min} = 460$ μm or $h = 10$ μm with h being the distance above the dielectric surface. It can be observed that in the absence of the axial magnetic field (dashed line) the electron hits the dielectric surface. For $B_0 = 8$ kGs (dotted line, the unit 1 $Gs = 10^{-4}$ T), the electron's x trajectory has a more confined structure but still will hit the dielectric. However, for a larger axial magnetic field of $B_0 = 10\,KG$ (solid line), the electron stays away from the dielectric with some oscillations.

In the simulations of Ref. [20] the axial magnetic field was taken as 8 kGs for the cylindrical waveguide and their results were not sensitive to the choice of magnetic field. Our results show that for the flat dielectric the proper value is $B_0 = 10$ kGs and it cannot be lower than that. In the cylindrical waveguide there is an azimuthal symmetry which gives a better confinement than the flat dielectric slab which is largely asymmetric in the x direction and therefore a relatively large axial magnetic field should be required.

In addition to the lower part of the beam, we also want to look at the top and the center of the electron beam. Figure 3 shows the variation of the position (x-component) of the lower part (solid line), central part (dashed line), and the top portion of the beam (dotted line) with the axial position z at $B_0 = 10$ kGs. The electron beam has a circular cross section on the x–y plane and the lower, central, and upper part of the beam are the points on the circle with minimum, maximum, and middle value of x, respectively. In fact, the lower part of the beam is the closest point to the dielectric surface. The electron on the top portion of the beam starts at $x_{\max} = 556$ μm where the electromagnetic field of radiation has 70% of its maximum strength on the surface of the dielectric at $x = 450$ μm. This top electron through some oscillations gradually and slowly moves away from the dielectric and reaches the point $x = 575$ μm with 65% of the radiation's maximum strength. It can be seen that all three parts of the electron beam move in a similar fashion and the shape and radius of the beam almost remain unchanged as beam moves through the dielectric.

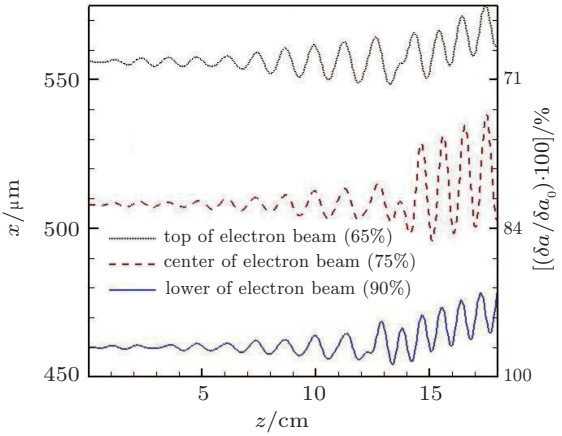


Fig. 3. Variation of x position (left axis), and percentage of vector potential amplitude with respect to its maximum value on dielectric surface (right axis), with axial position of the lower part (solid line), central part (dashed line), and top portion (dotted line) of beam with $B_0 = 10$ kGs.

Therefore, we conclude that for this set of parameters the optimum magnetic field is $B_0 = 10$ kGs and the lower part of the beam should be located at $x_{\min} = 460$ μm, which makes it located at 10 μm above the dielectric surface. Since the upper part of the beam is at $x_{\max} = 556$ μm this makes the radius of the electron beam be 48 μm. With this radius, the beam current should be around 8 mA to fulfil the condition $\omega_p \ll \omega$.

Figure 4 shows how the x–y transverse cross-section of the trajectory of the electron at lower part of the beam changes as the beam moves along the z axis. For $B_0 = 0$, the dotted line shows that the electron does not move along the y direction and has a wide span of movement along the x direction. The axial magnetic field $B_0 = 8$ kGs (dashed line) causes the electron to move in a helical shape trajectory with the radius of the cross-section being small at the injection point but increases gradually as the beam moves through the growing radiation. More effectively focusing is evident for the stronger magnetic field $B_0 = 10$ kGs (solid line). There is also a slight side shift of the trajectory in the y direction.

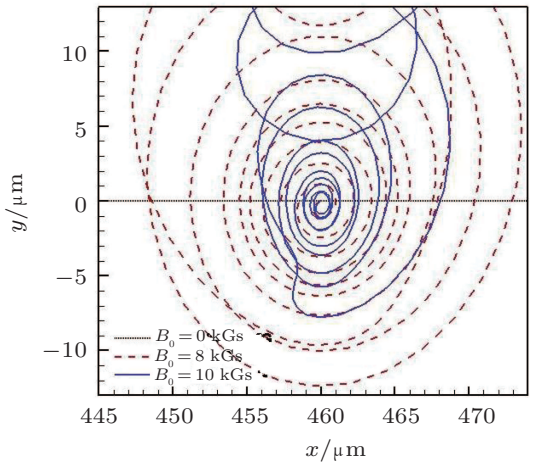


Fig. 4. Transverse cross-sections of the electron at lower part of beam respectively for $B_0 = 0$ kGs (dotted line), $B_0 = 8$ kGs (dashed line), and $B_0 = 10$ kGs (solid line).

3.2. High beam energy and high radiation growth

For the case of high beam energy, our parameters correspond to the analytical treatment in Ref. [16]. The flat dielectric is made of polyethylene with $\varepsilon = 2.2$ and with a thickness of 50 μm coated on a conductor. The initial beam energy is 2 MeV ($\gamma_0 = 5.01$) and the resonant frequency is 350 GHZ. In Ref. [16], the amplitude of the radiation starts from $\delta a = 10^{-7}$ and grows to $\delta a = 10^{-2}$ over a saturation length of 40 cm. This exponential growth is shown in Fig. 5(a).

Figure 5(b) shows the x positions of the electron at the lower part of the beam for different values of the axial magnetic field. This electron is injected at $x_{\min} = 100$ μm which is 50 μm above the dielectric surface. The solid line for $B_0 = 0$ indicates that the electron moves away from the interaction zone at the vicinity of the dielectric surface and completely moves out before reaching the saturation point at $z = 40$ cm. The dotted line for $B_0 = 30$ kGs exhibits that the electron is widely oscillating and therefore comes to contact the dielectric. For a strong magnetic field of 65 kGs (dashed line), due to its powerfully focusing effect, the electron neither hits the dielectric nor runs away from it.

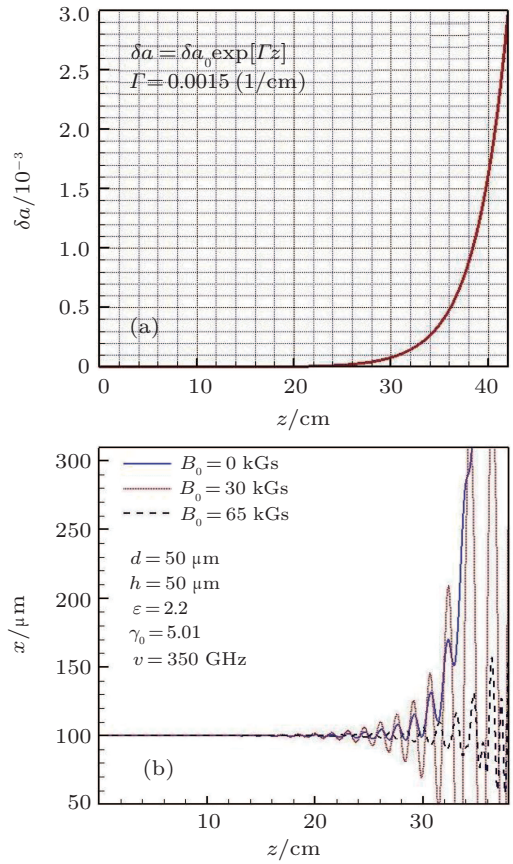


Fig. 5. (a) Exponential growth of vector potential varying with axial position z increasing at growth rate $\Gamma = 0.0015$ (1/cm), (b) x–z variation of electron at lower part of beam for different values of axial magnetic field.

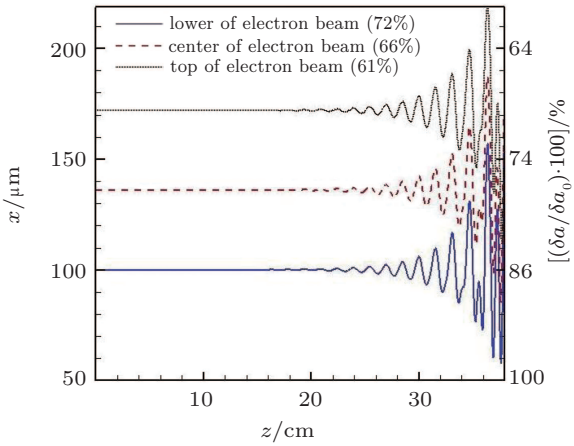


Fig. 6. Variation of x position (left axis), and percentage of vector potential amplitude with respect to its maximum value on dielectric surface (right axis), with axial position of lower part (solid line), central part (dashed line) and top portion (dotted line) of beam at $B_0 = 65$ kGs.

The variation of the position (x-component) of the lower part (solid line), central part (dashed line), and the top portion (dotted line) of the electron beam with the axial position z at $B_0 = 65$ kGs are shown in Fig. 6. It can be seen that for this choice of axial magnetic field the beam is not distorted and remains confined especially if the oscillations near the saturation point are averaged out. The average position of the electron at different points inside the electron beam almost remains at

their initial x position of the injection. Therefore, by remaining inside the interaction region, the electron beam is expected to strongly amplify the radiation. The initial position of the top of the beam at $x_{max} = 172\,\mu$m with 70% of the maximum amplitude of the radiation yields the initial radius of the beam, which is 36 μm. In this case, to fulfil the condition $\omega_p \ll \omega$, the current carried by the electron beam needs to be around 40 mA, which is consistent with the current and radius of the beam in Ref. [32].

We also try to show how we can reduce the necessary axial magnetic field by moving up the electron beam. In Fig. 7, the axial magnetic field is reduced to 50 KG while the case of$h = 50\,\mu$m is compared with the scenario of $h = 100\,\mu$m. It can be seen that for lower injection of the electron beam with $h = 50\,\mu$m (solid line), the electron will strike the dielectric surface but the higher injected electron at $h = 100\,\mu$m (dashed line) will stay well above the dielectric and it will not run away from the interaction zone. However, the problem with the higher injection at $h = 100\,\mu$m is that the electron beam will move up and enter into the weaker interaction zone unless the beam size is reduced to an unacceptably small radius. Therefore, it is concluded that the lowest possible axial magnetic field, for this set of parameters for a high beam energy, is 65 kGs.

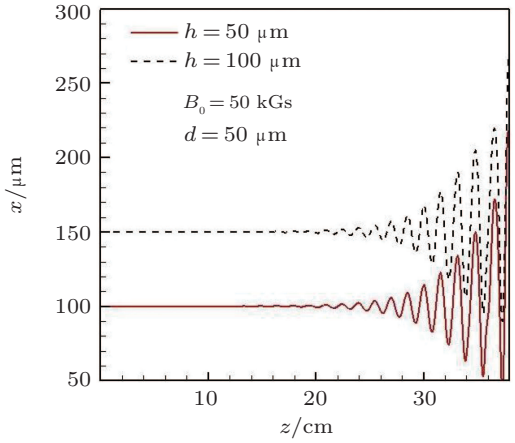


Fig. 7. Variations of x of electron at lower part of beam with axial position for different values of electron injections.

3.3. Low energy beam and high radiation growth

In Ref. [16], high radiation growth of 10^5 was also reported for low energy electron beam of $\gamma = 2$. However, it differs from the case of the high energy beam of $\gamma = 5$ by the fact that it has a much shorter saturation length. Therefore, in our third investigation, for the low energy beam and high radiation growth, we take the parameters from the simulation in Ref. [13] (used in the Dartmouth experiment[32]) which has low electron beam energy of 30 keV ($\gamma = 1.07$). However, since in this simulation the CFEL is in the oscillator mode we take the radiation growth of 10^5, for δa, over the saturation length of 20 cm from Ref. [16]. This radiation growth is shown in Fig. 8(a). For the dielectric structure and the electron beam of the simulation in Ref. Ref. [13], we investigate the trajectory of an electron at the lowest part of the electron beam in the x–z plane in Fig. 8(b), for different axial magnetic fields. The flat dielectric is made of GaAs with dielectric constant $\varepsilon = 13.1$ and thickness $d = 350\,\mu$m. The electron is injected at $x_{min} = 351\,\mu$m which is 1 μm above the dielectric surface. The solid line shows that in the absence of axial magnetic field the electron, by going through oscillations in the x-direction, will hit the dielectric surface midway through the path. For $B_0 = 10$ kGs (dashed line), the electron moves away from the interaction zone before reaching the saturation point. However, for the stronger magnetic field of $B_0 = 20$ kGs (dotted line) although the electron drifts away from the dielectric, it remains well within the interaction zone.

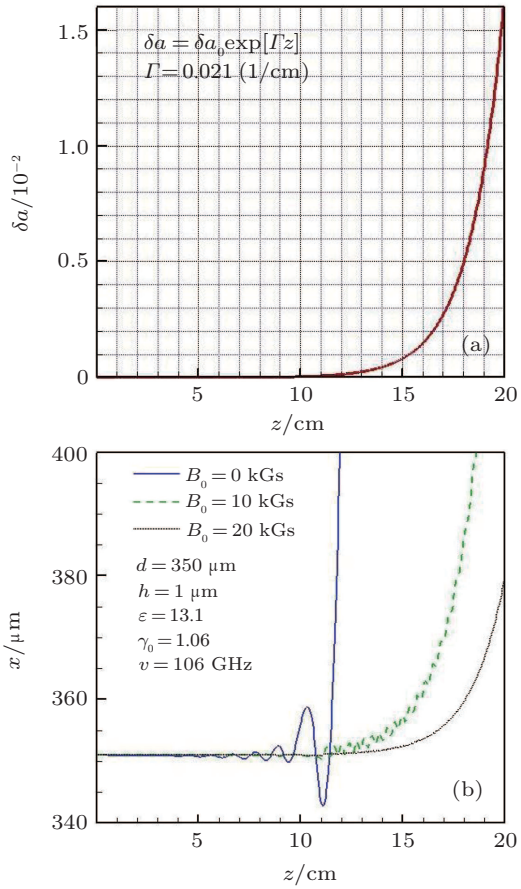


Fig. 8. (a) Exponential growth of vector potential along z axis at $\Gamma = 0.021$ (1/cm), and (b) x–z variation of the electron at lower part of beam for different values of axial magnetic field.

The variation of the position (x-component) of the lower part (solid line), the central part (dashed line), and the top portion (dotted line) of the electron beam with axial position z at $B_0 = 20$ kGs are shown in Fig. 9. It can be seen that except for the approximately 30 μm upward drift, the electron beam remains focused and is not disturbed. The upper part of the

electron beam moves to a position around $x = 430$ μm where it experiences 53% of the maximum strength of the radiation at the saturation point. Therefore, by remaining a great part of radiation inside the interaction region, the electron beam is expected to strongly amplify the radiation. The initial position of the top of the beam at $x_{\max} = 401$ μm with 70% of the maximum amplitude of the radiation yields the initial radius of the beam, which is 25 μm. In this case, to fulfil the condition $\omega_p \ll \omega$ the current needs to be around 1 mA.

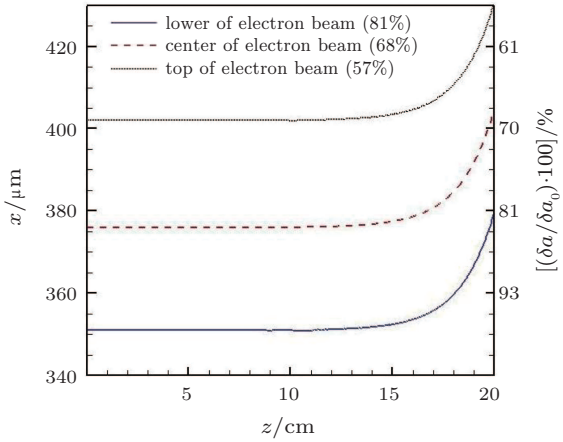


Fig. 9. Variation of x position (left axis), and percentage of vector potential amplitude with respect to its maximum value on dielectric surface (right axis), with axial position of lower part (solid line), central part (dashed line) and top portion (dotted line) of beam at $B_0 = 20$ kGs.

Figure 10 shows the change in electron energy for the lower part of the electron beam, indicating that the electron loses energy as it moves along the z axis over the dielectric surface. This energy is actually converted into the growing radiation. This change in the electron's energy is lowest for $B_0 = 0$ and is highest for $B_0 = 20$ kGs because the strong magnetic field keeps the electron focused and confines it well in the interaction region thereby allowing it to amplify the radiation.

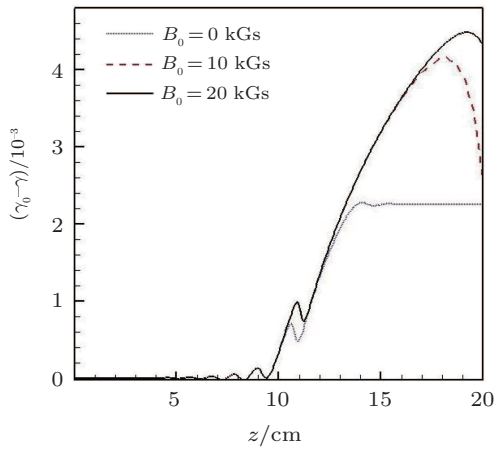


Fig. 10. The electron energy varying along the z axis for different values of axial magnetic field.

We anticipate, on the physical ground, that in CFELs with low output power,[32,39] the electron beam will not be influenced much by the radiation. In this regime, radiation is not strong enough to deviate the electron beam away from the interaction zone. It can be seen in Figs. 5 and 8 that as long as the dimensionless amplitude of a radiation $\delta a$is less than 10^{-4}, there are not many oscillations in the electron beam moving in the x direction, even in the absence of the axial magnetic field.

In the conventional FEL, the electrons move through a wiggler magnetic field in steady-state orbits in the absence of radiation.[42] These steady-state trajectories that are perturbed in the presence of radiation, form the bases of many analytical studies of FELs. These studies are possible because the bunching of the electron beam is due to the coupling between the steady-state trajectories and the radiation. In the CFEL, however, there is no separate wiggler field but rather bunching of the electron beam takes place because of the longitudinal electric field of the TM mode of the radiation. Here is the picture: as the electron beam moves along the radiation its bunching with the longitudinal electric field amplifies the radiation. Since the agent responsible for the bunching is itself part of the growing radiation, the analytical solution for the single particle equations of motion is not possible even in the case of a small amplitude radiation, and they need to be solved numerically. For this physical reason, these equations cannot be solved analytically under any justifiable simplifying assumption.

In Refs. [19] and [20], self-consistent simulations of CFEL were presented for a dielectric cylindrical waveguide in the presence of a focused axial magnetic field. They solved the equation of motion of the electrons in the presence of the radiation numerically and found interesting results in agreement with the corresponding experimental results. They found that their results were not sensitive to an axial magnetic field. The reason is that the waveguide provides additional focusing for the electron beam, thereby preventing the electrons from hitting the waveguide wall.

We find in the present analysis that in the high power CFEL with a flat dielectric slab, an axial magnetic field is necessary and the injection position of the electron beam relative to the dielectric surface needs to be determined for its effective interaction with the radiation. The highly asymmetric nature of this problem is the plausible physical reason for requiring an axial magnetic field. The electron beam faces the dielectric surface on one side and experiences the vacuum with declining radiation on the other side. We find that an axial magnetic field is necessary to keep the electron beam confined and prevent it from either hitting the dielectric slab on one side or moving out of the interaction region on the other side. The interaction process is considered to be in the exponential growth, which takes place in the linear regime. Therefore, the growth rate is

considered to be constant and it is determined by the strength of the radiation at saturation and the saturation rate.

4. Conclusions

In this paper, the motion of a single electron in a single slab CFEL is used to find an optimal electron beam for the effective interaction with the growing electromagnetic radiation. Assuming a growth rate for the radiation, the equations of motion of the electrons are solved numerically to find the trajectories of electrons in the interaction plane. It is found that an axial magnetic field is always necessary to keep the electron beam in the interaction zone for the high output power. This analysis is in agreement with two previous numerical studies for a cylindrical waveguide[19,20] but is at odds with analytical treatments of a flat dielectric in which there was used no axial magnetic field.[16] This is backed by an interesting physical reason. Furthermore, the required conditions for preventing the electrons from striking the dielectric surface are obtained and discussed. This gives us a minimum distance between the electron beam and the dielectric slab. Since the radiation weakens exponentially as the electron beam is moved away from the dielectric slab, the maximum distance between the electron beam and the dielectric slab is also determined in order to prevent the electrons from moving far from the slab and moving out of the interaction region above the dielectric. These minimum and maximum distance give the optimal radius of the electron beam. The beam radius and the parameters of the dielectric are used to find the electron beam current that satisfies the condition $\omega_p \ll \omega$ and, therefore, gives negligible space-charge effect.

The analysis is carried out for three different sets of parameters and it is always found that an axial magnetic field is necessary to keep the electron beam focused for the high output power. In the first set of parameters the suitable axial magnetic field is consistent with what was used in Ref. [20].

References

[1] Perenzoni M and Paul D J 2014 *Physics and Applications of Terahertz Radiation* (Springer)
[2] Weide D V D 2003 *Opt. Photon. News* **14** 48
[3] Ciocci F, Dattoli G, De Angelis A, et al. 1987 *Nucl. Instrum. Methods Phys. Res. A* **259** 128
[4] Ciocci F, Doria A, Gallerano G P, Giabbai I, Kimmitt M F, Messina G, Renieri A and Walsh J E 1991 *Phys. Rev. Lett.* **66** 699
[5] Garate E, Cook R, Heim P, Layman R and Walsh J 1985 *J. Appl. Phys.* **58** 627
[6] Garate E, Shaughnessy C and Walsh J 1987 *IEEE J. Quantum Electron.* **23** 1627
[7] Garate E P, Moustaizis S, Buzzi J M, Rouille C and Lamain H 1986 *Appl. Phys. Lett.* **48** 1326
[8] Walsh J and Murphy J 1982 *IEEE J. Quantum Electron.* **18** 1259
[9] Liu F, Xiao L, Ye Y, Wang M, Cui K, Feng X, Zhang W and Huang Y 2017 *Nat. Photon.* **11** 289
[10] Asgekar V B and Dattoli G 2005 *Opt. Commun.* **255** 309
[11] Ciocci F, Dattoli G, Doria A, Gallerano G P, Schettini G, Toree A E D, Auston D, Jacobs R, Bartolini R and Liao P 1987 in *Conference on Lasers and Electro-Optics*, Baltimore, Maryland, OSA, USA
[12] Gallerano G P, Doria A, Giovenale E and Renieri A 1999 *Infrared Phys. Technol.* **40** 161
[13] Kalkal Y and Kumar V 2015 *Phys. Rev. ST Accel. Beams* **18** 030707
[14] Wiggins S M, Jaroszynski D A, McNeil B W J, Robb G R M, Aitken P, Phelps A D R, Cross A W, Ronald K, Ginzburg N S, Shpak V G, Yalandin M I, Shunailov S A and Ulmaskulov M R 2000 *Phys. Rev. Lett.* **84** 2393
[15] Fares H and Yamada M 2011 *Phys. Plasmas* **18** 093106
[16] Gore B W and Asgekar V B 1996 *Phys. Scr.* **53** 62
[17] Li D, Huo G, Imasaki K, Asakawa M and Tsunawaki Y 2010 *Infrared Phys. Technol.* **53** 204
[18] Sharma G and Mishra G 2012 *Nucl. Instrum. Methods Phys. Res. A* **685** 35
[19] Freund H P 1990 *Phys. Rev. Lett.* **65** 2993
[20] Freund H P and Ganguly A K 1990 *Phys. Fluids B* **2** 2506
[21] Li D, Wang Y, Hangyo M, Wei Y Z, Yang and Miyamoto S 2014 *Appl. Phys. Lett.* **104** 194102
[22] Wang Y, Wei Y, Li D, Takano K, Nakajima M, Jiang X, Tang X, Shi X, Gong Y, Feng J and Miyamoto S 2015 *Phys. Plasmas* **22** 083111
[23] Wang Y, Wei Y, Li D, Wanghe W, Xianbao S, Xia L, Qian L, Hairong Y, Jin X, Luqi Z, Chong D, Yubin G and Wenxiang W 2016 in *IEEE International Vacuum Electronics Conference (IVEC)*
[24] Kalkal Y and Kumar V 2016 *Nucl. Instrum. Methods Phys. Res. A* **827** 85
[25] Fares H 2012 *Nucl. Instrum. Methods Phys. Res. A* **690** 111
[26] Cao M M, Liu W X, Wang Y and Li K 2014 *Acta Phys. Sin.* **63** 024101
[27] Cao M M, Liu W X, Wang Y and Li K 2016 *Acta Phys. Sin.* **65** 014101
[28] Ye Y, Liu F, Cui K, Feng X, Zhang W and Huang Y 2018 *Opt. Express* **26** 31402
[29] Li M, Yang X F, Xu Z, *et al.* 2018 *Acta Phys. Sin.* **67** 084102
[30] Lin X L, Zhang J B, Lu Y, Luo F, Lu S L, Yu T M and Dai Z M 2010 *Chin. Phys. Lett.* **27** 044101
[31] Li W, Jiang S, He Z, Jia Q, Wang L and He D D 2018 in 9*th International Particle Accelerator Conference*, Canada, JACoW
[32] Owens I J and Brownell J H 2005 *J. Appl. Phys* **97** 104915
[33] Weatherall J C and Main W 1992 *Phys. Fluids B* **4** 1953
[34] Main W T, Garate E, Weatherall J C and Cherry R 1992 *IEEE T. Plasma Sci.* **20** 281
[35] Asgekar V B and Dattoli G 2002 *Opt. Commun.* **206** 373
[36] Fares H, Yamada M and Kuwamura Y 2010 *Jpn. J. Appl. Phys.* **49** 096402
[37] de la Fuente I, van der Slot P J M and Boller K J 2007 *Phys. Rev. ST Accel. Beams* **10** 020702
[38] Fares H 2012 *Phys. Plasmas* **19** 053109
[39] Kalkal Y and Kumar V 2016 *Phys. Rev. Accel. Beams* **19** 060702
[40] Yatsenko T, Ilyenko K and Sotnikov G V 2012 *Phys. Plasmas* **19** 063107
[41] Hill N, Vaughan W, Price A H and Davies M 1969 *Dielectric Properties and Molecular behaviour* (London: Van Nostrand Reinhold)
[42] Freund H P and Antonsen T M 1992 *Principles of free-electron laser* (London: Chapman-Hall), Chap. 2